Acta Geodyn. Geomater., Vol. 23, No. 2 (222), 207–221, 2026
DOI: 10.13168/AGG.2026.0013
journal homepage: https://www.irsm.cas.cz/acta

ORIGINAL PAPER

CHANGES IN ROCK MECHANICAL PROPERTIES DUE TO HIGH TEMPERATURES: A NATIONWIDE STUDY IN THE CZECH REPUBLIC, CENTRAL EUROPE

Ghazaal RASTJOO [1, 2], Marco LOCHE [1,2], Ondřej RACEK [1], Xuan-Xinh NGUYEN [1], Artem POLEZHAEV [1] and Jan BLAHŮT [1] *

[1] *Institute of Rock Structure and Mechanics, Czech Academy of Sciences, V Holešovičkách 41, 182 09 Prague, Czech Republic*
[2] *Institute of Hydrogeology, Engineering Geology and Applied Geophysics, Charles University, Albertov 6, 128 43 Prague, Czech Republic*

**Corresponding author's e-mail:* blahut@irsm.cas.cz

ARTICLE INFO

Article history:
Received 15 February 2026
Accepted 17 March 2026
Available online 17 March 2026

Keywords:
Thermal damage mechanism
Physico-mechanical properties
Igneous and metamorphic rock
Sandstone, Limestone
Volcanic rock

ABSTRACT

Wildfires are becoming increasingly frequent and intense due to ongoing climate change, affecting not only ecosystems but also the stability and integrity of rock masses in fire-prone landscapes. High temperatures associated with wildfires can alter the physical and mechanical properties of rock faces, with significant implications for slope stability, weathering rates, and landscape evolution in affected regions. In this study, we investigated the effects of thermal shock on rock mechanical properties in four lithological groups: igneous and metamorphic rocks, sandstones, limestones, and volcanic rocks. For each group, samples were collected from 25 different locations across the Czech Republic, Central Europe to provide a representative dataset covering the regional geological diversity. Specimens were subjected to fast short-term heating at target temperatures (from 105 °C to 800 °C). After each heating step, changes in the propagation velocities of Vp and Vs were measured, allowing the calculation of dynamic elastic moduli. Our results reveal markedly different thermal responses across lithological groups. In several cases, a surprising increase in wave velocity was observed after heating to 200 °C. However, higher temperature exposures generally resulted in progressive degradation of material properties, including a sharp decrease in tensile and uniaxial compressive strength and Mode I fracture toughness. These findings highlight the complex and non-linear nature of thermal alteration in rocks and stress the importance of considering lithology-specific behaviour when assessing post-fire landscape stability and rock mass quality. Our results contribute to a better understanding of how wildfires, intensified by climate change, may accelerate rock degradation processes and reshape geomorphological systems.

1. INTRODUCTION

Over the past few decades, patterns of wildfire activity have undergone significant changes due to the ongoing climate crisis, resulting in profound impacts on both populations and economies in many countries (McCaffrey, 2004; Moreira et al., 2011). Regions that have historically not experienced extreme hazards, such as wildfires, droughts, and prolonged dry spells, are now increasingly exposed to such processes. These hazards are expected to grow in severity with the anticipated increase in wildfire frequency and intensity. Despite this trend, the physical implications of these changes, particularly concerning mechanical and thermo-hydro-mechanical responses of geomaterials, remain underexplored (Scaringi and Loche, 2022).

The link between wildfires and mass wasting events stems from the transformative impact that fires have on the physical properties of rocks. During a wildfire, the high temperatures can cause thermal cracking and rock mass alteration, leading to, a decrease in strength, and increased susceptibility to mechanical failure (Nyman et al., 2019; Buckman et al., 2021). The fire-induced heating of rocks can have, as its main macroscopic effect, rock spalling, resulting in increased weathering and sediment supply, as well as changes in rock physico-mechanical properties.

As climate models predict an increase in wildfires and dry spells in the future, thus understanding these relationships is becoming urgent. For instance, in 2022, a devastating wildfire hit the Czech Republic (Hruška et al., 2022; Kudláčková et al., 2024). This event shed light on the emerging frequency of forest fires in higher latitudes such as the Czech Republic, as highlighted by several authors (Hillayová et al., 2023; Trnka et al., 2021; Dupuy et al., 2020; Ruffault et al., 2020; Shtober-Zisu and Wittenberg, 2021a; Yıldız et al., 2023; Loche et al., 2026), and thus leading to a higher likelihood of affected rock masses (Hlásný et al., 2014; Schelhaas et al., 2010; Filippi et al., 2026).

In this perspective, it is crucial to investigate the response of diverse lithologies. Notably, analyses are generally focused on evaluating single lithotypes and adopting thermal treatments on cylindrical rock samples (Goudie et al., 1992; Dorn, 2003; Sarro et al., 2021; Shtober-Zisu and Wittenberg, 2021a, 2021b). However, it is beneficial to quantify the response of

Cite this article as: Rastjoo G, Loche M, Racek O, Nguyen X-X, Polezhaev A, Blahůt J: Changes in rock properties due to high temperatures: A nationwide study in the Czech Republic, Central Europe. Acta Geodyn. Geomater., 23, No. 2 (222), 207–271, 2026. DOI: 10.13168/AGG.2026.0013

each rock type following a temperature shock (Lainas et al., 2021). The impact of fire temperature on mineral composition and crystal structure has already been discussed in previous studies (Aboayanah et al., 2024; Kompaníková et al., 2014; Ram et al., 2025). Research on sandstone materials indicates resistance to cracking at temperatures up to 400 °C, while mineral transformations and physical changes are associated with superficial Fe reactions observed above 300 °C. On the other hand, studies on granite show that thermal crack density and aperture increase with pre-treatment temperature, significantly affecting the thermal cracking pattern under subsequent gradient heating. This suggests a transition in thermomechanical behaviour between 300 and 500 °C. The samples are thus sensitive to heating strategies, and attention should be given to artificial oven testing to better account for the natural heterogeneity of rocks and lithologies (Řimnáčová et al., 2024).

Given the profound link between Brazilian tensile strength (*BTS*), which governs rock spalling and rockfall development, and fire-prone materials, we have chosen to use Brazilian samples (Zhao et al., 2018). Parallelly, classical uniaxial compressive tests (*UCS*) have been performed to represent and derive the *UCS* and Fracture toughness samples (*FT*), which were utilised to evaluate Mode I fracture toughness. In parallel, non-destructive techniques have been employed as a practical tool for providing an analysis of even disturbed samples (Goudie, 1999; Yeste-Lizán et al., 2023).

In this study, we investigated the effects of rapid thermal shock on rock mechanical properties, with destructive and non-destructive techniques, in four lithological groups: igneous and metamorphic, sandstones, limestones and volcanic rocks. For each lithological group, samples were collected from 25 different locations across the Czech Republic, Central Europe to provide a representative and statistically robust dataset covering the region's geological diversity (Dally, 2008; Gill et al., 2005).

2. MATERIALS AND METHODS

The territory of the Czech Republic comprises a variety of lithological groups and a complex geological evolution. Most of the country is dominated by the Bohemian Massif, whose Variscan basement comprises granitoids, gneiss, migmatites, and amphibolite rocks of Proterozoic and Palaeozoic age. Younger sedimentary rocks overlay the basement, mostly in the central and northern parts (Matula and Pašek, 1986). The Bohemian Karst in the Central part of the Czech Republic is composed of Palaeozoic limestones, similar to the other limestone area of Moravian Karst in the southeast of the country. A large part of central and northern part of the Czech Republic is formed by the Bohemian Cretaceous Basin, where thick sandstone layers have developed into peculiar rock formations, including "sandstone cities" (Svoboda et al., 1966). In the north-western part of the country, Tertiary volcanic rocks are present. The flysch zone of the Outer Western Carpathians (Alpine-Himalayan orogeny) dominates the eastern part of the Czech Republic (Chlupáč et al., 2002).

To capture the large geological variety of the Czech Republic in relation to existing rock slopes that may have been affected by wildfires, we used the engineering-geological map at 1: 500 000 (Fig. 1) (https://mapy.geology.cz/arcgis/rest/services/Geohazardy/IG_rajony500/MapServer), which is divided into a number of classes that reflect the engineering-geological properties of the rocks. Taking into account the presence of rock outcrops and rock slopes that might be affected by the wildfires, the classes were grouped into four categories: (i) igneous and metamorphic rocks; (ii) sandstones; (iii) limestones; and (iv) volcanic rocks (Fig. 1). The areas of the different lithological groups are varied, but this selection and grouping allowed us to gather information about the large variety of existing outcrops and rock walls, including those located in protected areas. The remaining areas were excluded from sampling as they mostly represent soils and soft rocks, which usually do not form rock outcrops and steep, rockfall susceptible rock slopes.

For each lithological rock group, 25 samples were collected to allow robust statistical analysis and comparison of the selected lithological groups. From each of these samples, five BTS, two UCS, and three FT specimens were prepared (Fig. 2). All of the prepared specimens (1000 pieces in total) were vacuum-saturated in water for 24 hours under -1 atm pressure to ensure complete saturation of pores, after which their saturated weights were recorded to calculate effective porosity. Subsequently, the specimens were oven-dried at 105 °C for 24 hours, following the ISRM recommended Methods (Ulusay and Hudson, 2007). After cooling at room temperature, the specimens were measured, weighed, and their bulk density was calculated. They were kept in a desiccator to prevent moisture from entering the specimens. After drying, the ultrasonic pulse velocity (UPV) test was performed on all BTS and UCS specimens to assess their initial conditions and changes during the testing. We remind that for the FT ultrasonic test was not possible given the peculiar geometry. However, UPV was selected as a standard non-destructive technique, allowing for the determination of dynamic elastic moduli of the BTS and UCS specimens.

Laboratory UPV employed two pairs of Olympus resonant ultrasonic sensors (V103 for P-waves, V153 for S-waves) with a resonant frequency of 1 MHz, where the distance between the centres of the transducers was kept at a constant of 25 mm in BTS and 100 mm in UCS. Based on the experimentally determined wave velocities, it was possible to calculate some principal dynamic elastic parameters such as Young's modulus (*Ed*), shear modulus (*Ud*), Poisson's ratio (*Vd*) and bulk modulus (*Kd*) (Schön, 2015).

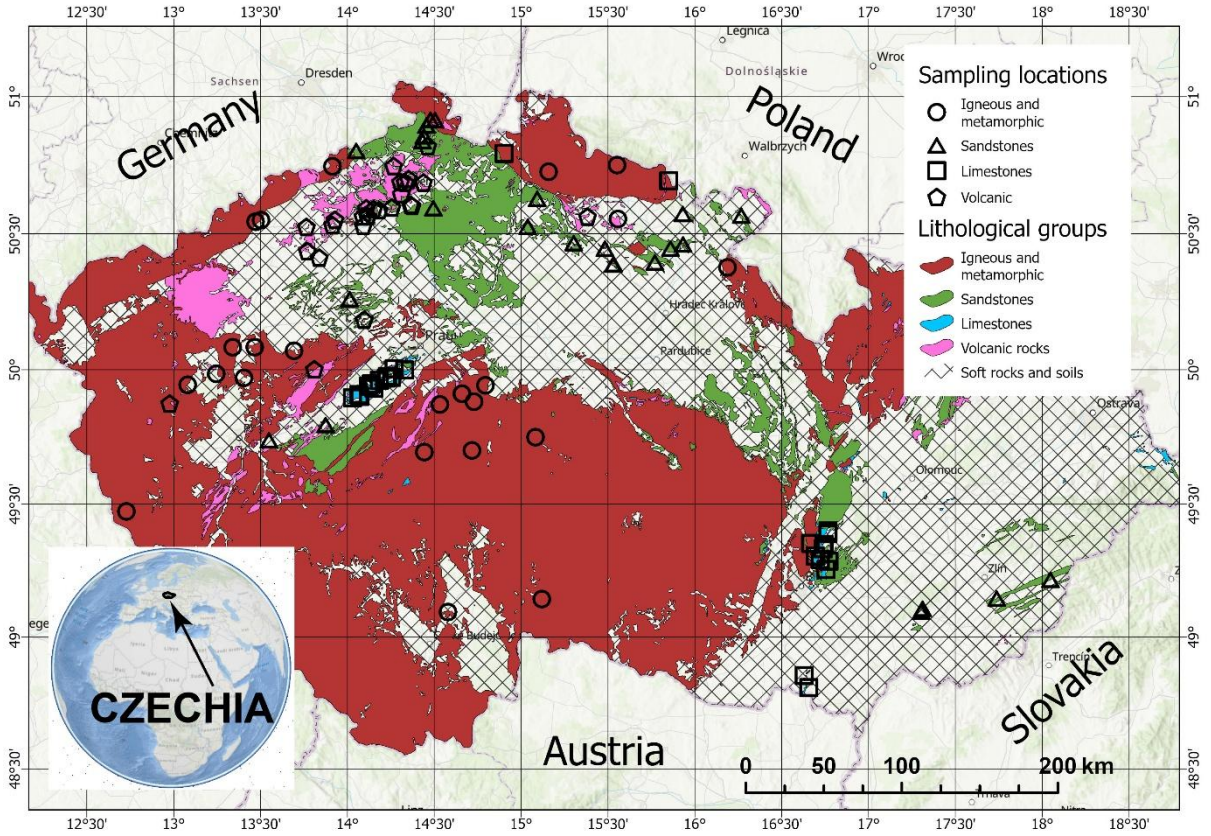

Fig. 1 Study location and sampling sites across the Czech Republic. The map shows the extensive sampling locations of the four lithological units, along with their relative correspondence and coverage within the associated lithological groups. The inset presents the global location of the Czech Republic in Central Europe.

The dried specimens were exposed to a controlled rapid thermal treatment using a programmable laboratory furnace (CLASIC 1013). This allowed the investigation of controlled repeated heating and thermal fatigue. BTS specimens were thus subjected to four short-term heating phases at target temperatures of 200 °C, 400 °C, 600 °C, and 800 °C. A steady heating rate of 100 °C/min was used, and specimens were held at each target temperature for 5 minutes to ensure uniform thermal distribution before cooling naturally to room temperature. Following each heating stage, UPV tests were performed on the specimens, enabling the assessment of changes in their dynamic elastic moduli. Similarly, the UCS was tested for 200 °C, 400 °C, 600 °C, 800 °C, while the FT, given they restrict number of samples were heated to 350 °C, and 600 °C. Finally, specimens at each target temperature were tested to determine their corresponding tensile strength, uniaxial strength and Mode I fracture toughness (ISRM, 1978).

For BTS, tests were performed on the prepared thermally treated rock specimens with the load applied continuously at a constant displacement rate until failure. The maximum load at failure was recorded and converted to tensile strength using equation 1:

$$\sigma_t = 0.636 * \frac{P_{max}BTS}{Dt} \quad (1)$$

where σ_t is the calculated tensile strength, P_{maxBTS} is the maximum recorded load, D is the sample diameter, t is the sample thickness, according to ISRM standard (ISRM, 1978).

While it is known that the peak BTS values usually overestimate the true tensile strength (Packulak et al. 2025), the BTS test was selected because of its ease of implementation for a large number of specimens (500 in total).

For UCS, the peak axial load at failure was recorded during the unconfined compression test and converted to uniaxial compressive strength using equation 2:

$$\sigma_c = \frac{P_{max}UCS}{A} \quad (2)$$

where σc is the calculated compressive strength, P_{maxUCS} is the maximum load sustained by the specimen, and A is the initial cross-sectional area perpendicular to the loading direction (Bieniawski and Bernede, 1979). Although UCS testing requires careful specimen preparation to meet geometric tolerances, it remains the standard method for characterising the compressive strength of intact rock due to its straightforward interpretation and widespread acceptance in rock mechanics.

The fracture toughness method was selected because it enables reliable estimates of Mode I crack

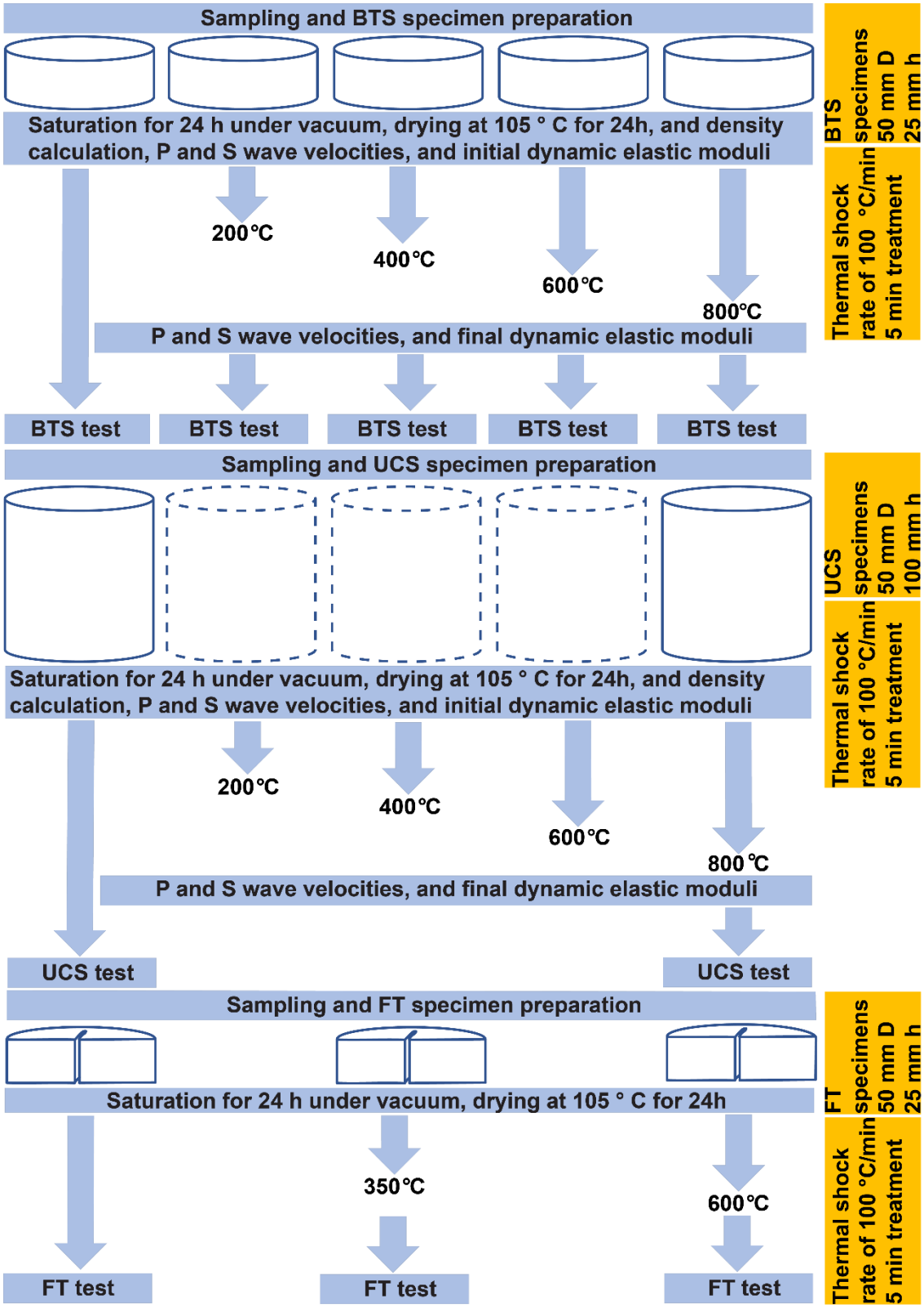

Fig. 2 Methodological framework of the study for BTS, UCS and FT.

initiation resistance. It was determined from the peak load measured during the semi-circular bend test and converted to Mode I fracture toughness using equation 3:

$$K_{IC} = \frac{P_{maxFT}\sqrt{\pi a}}{2RB} * \mathrm{Y(a)} \quad (3)$$

where K_{IC} is the calculated fracture toughness, P_{maxFT} is the maximum applied load, R is the radius of the specimen, B is the thickness, a is the notch length, and $Y(a)$ is the normalised geometry factor (Kuruppu et al., 2014).

In this study, only changes of mechanical properties were analysed, as the widespread nature of the study did not allow for detailed thin-section analysis of the mineralogical changes of the samples, which was also not the main aim of the study.

3. RESULTS

3.1. NON-DESTRUCTIVE TESTING

In this section, we present the experimental results of the thermally treated *BTS* and *UCS* specimens, with focus on P-wave (Vp) and S-wave (Vs) and their velocity decrease trend. Additionally, results on the computed dynamic elastic moduli are presented in the **Supplementary Materials (Figs. S1- 2)**.

3.1.1. BTS SPECIMENS

For igneous and metamorphic rocks, both Vp and Vs show a decrease with increasing treatment temperature. Vp values decline gradually up to 400 °C, followed by a sharper drop between 400 °C and 800 °C, with most values reaching around 40–60 % of the initial velocity (Fig. 3). Vs values follow a similar trend, although the reduction is slightly more gradual, with values at 800 °C stabilising between 30–50 % of the original value.

In sandstones, the initial Vp values are near 3 km/s and remain relatively stable up to 200 °C (Fig. 3). Beyond this temperature, a progressive decrease is observed, reaching approximately 50–70 % of the starting value at 800 °C. Vs velocities display a more gradual decline, with moderate dispersion among data, particularly beyond 400 °C. At 800 °C, Vs velocities typically range between 40–60 % of the initial values.

For limestones, Vp velocities start near 6 km/s and decline steadily with increasing temperature, showing a more linear reduction compared to crystalline rocks and sandstones. At 800 °C, most samples retain between 60–80 % of their initial Vp velocity, indicating lower thermal sensitivity in this velocity mode (Fig. 3). Vs velocities decrease more noticeably, particularly beyond 400 °C, with final values at 800 °C around 50–70 % of the original. The spread among data is greater for Vs, showing that thermal treatments affected shear wave propagation in limestone more than compressional wave propagation.

Volcanic rocks display the most variable response to thermal treatment. Vp velocity values remain close to initial up to 200 °C, after which they decrease irregularly, with some samples maintaining over 80 % of original velocity even at 800 °C and others dropping to nearly 50 %. Vs values show a similarly inconsistent decline, with significant divergence between samples at high temperatures. At 800 °C, Vs velocities range from approximately 40 % to 80 % of the original values (Fig. 3).

3.1.2. UCS SPECIMENS

In igneous and metamorphic rocks, both Vp and Vs exhibit a monotonic velocity decrease with increasing temperature. Vp values remain relatively stable between 105 °C and 200 °C, after which a progressive decline starts. The reduction intensifies beyond 400 °C, and by 800 °C, most samples fall to roughly half of their initial velocity. Vs follows the same general trend, but with slightly greater sensitivity and values at 800 °C commonly lie well below those of Vp for the same temperature steps.

Sandstones show comparatively stable Vp values up to 200 °C, after which a gradual decline begins. By 800 °C, Vp typically reaches about half of the initial velocity, though variability among samples increases at higher temperatures. Vs decreases more progressively, with a noticeable spread emerging beyond 400 °C; final values at 800 °C generally fall between 40–60°% of the initial state.

Limestones display a more linear and moderate reduction in Vp compared to the other lithologies. Vp decreases steadily with temperature, yet even at 800 °C, many samples retain 60–80 % of their initial velocity values, indicating comparatively lower thermal sensitivity. Vs, however, shows a stronger response with a decline accelerating beyond 400 °C, and values at 800 °C commonly fall to around 50–70 % of the initial velocity, with greater dispersion than observed for Vp.

Volcanic rocks exhibit the highest variability across all measured parameters. Vp remains close to initial values up to 200 °C, but the response becomes irregular at higher temperatures. Samples maintain more than 80°% of their initial velocity at 800 °C, while others drop to around 50 %. Vs shows a similarly heterogeneous pattern, with divergence between samples increasing markedly above 400 °C and final values at 800 °C range broadly from 40°% to 80°%.

3.2. DESTRUCTIVE TESTING

In this section, we present the experimental results of the thermally treated *BTS*, *UCS*, and *FT* specimens, with attention to their strength reduction. The different strength response (σ_t, σ_c and K_{IC}) permit the evaluation of the capacity of the samples to sustain stresses and resist failure under diverse target temperatures.

3.2.1. BTS SPECIMENS

Figure 5 shows the tensile strength in igneous and metamorphic rocks, which mirrors the previous patterns, with an initial constant value at 105 °C,

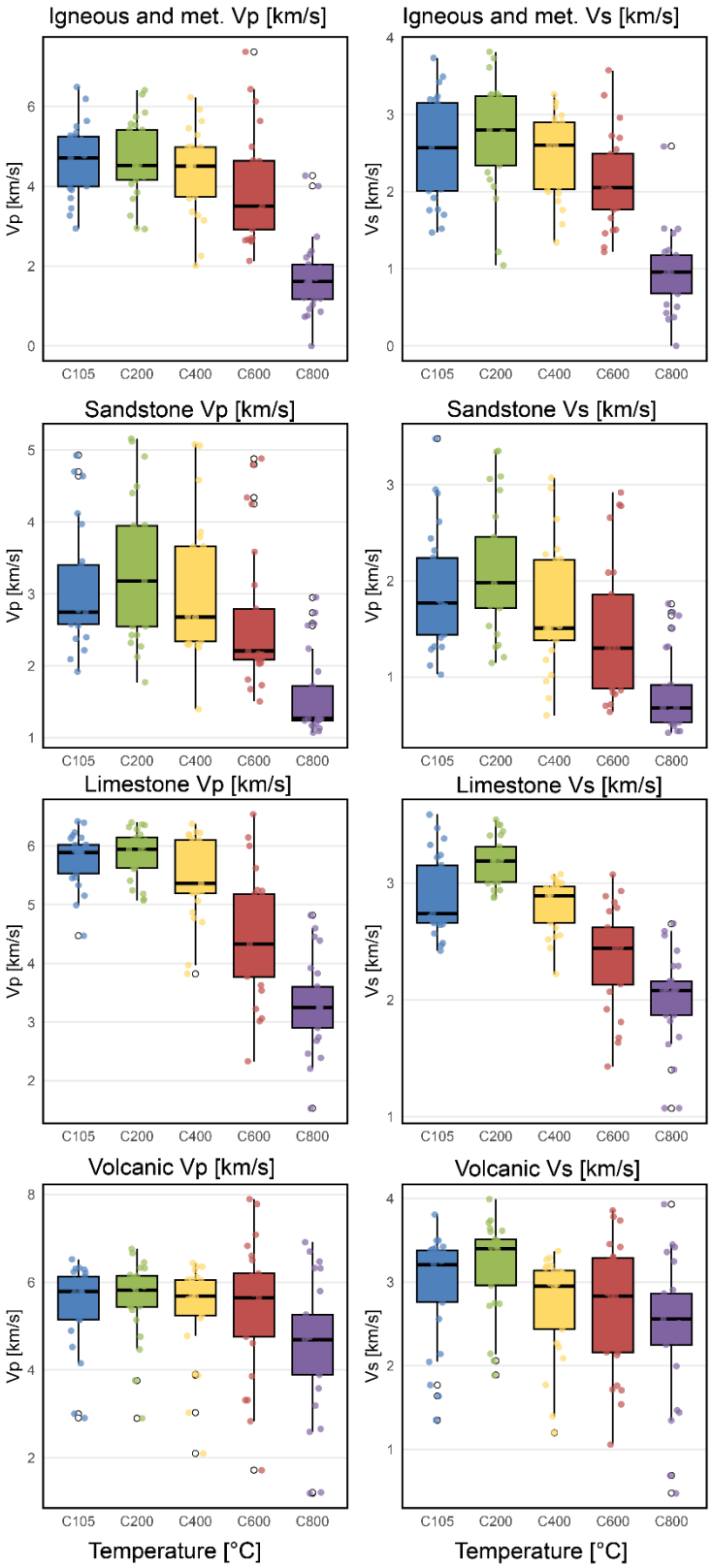

Fig. 3 Vp and Vs velocities of thermally treated BTS specimens of igneous and metamorphic, sandstone, limestone, and volcanic rocks were measured at five temperature levels (from 105 °C to 800 °C). Boxplots show the distribution of velocities for each rock type and temperature condition, highlighting the progressive thermal degradation and the contrasting sensitivity of different lithologies to heating.

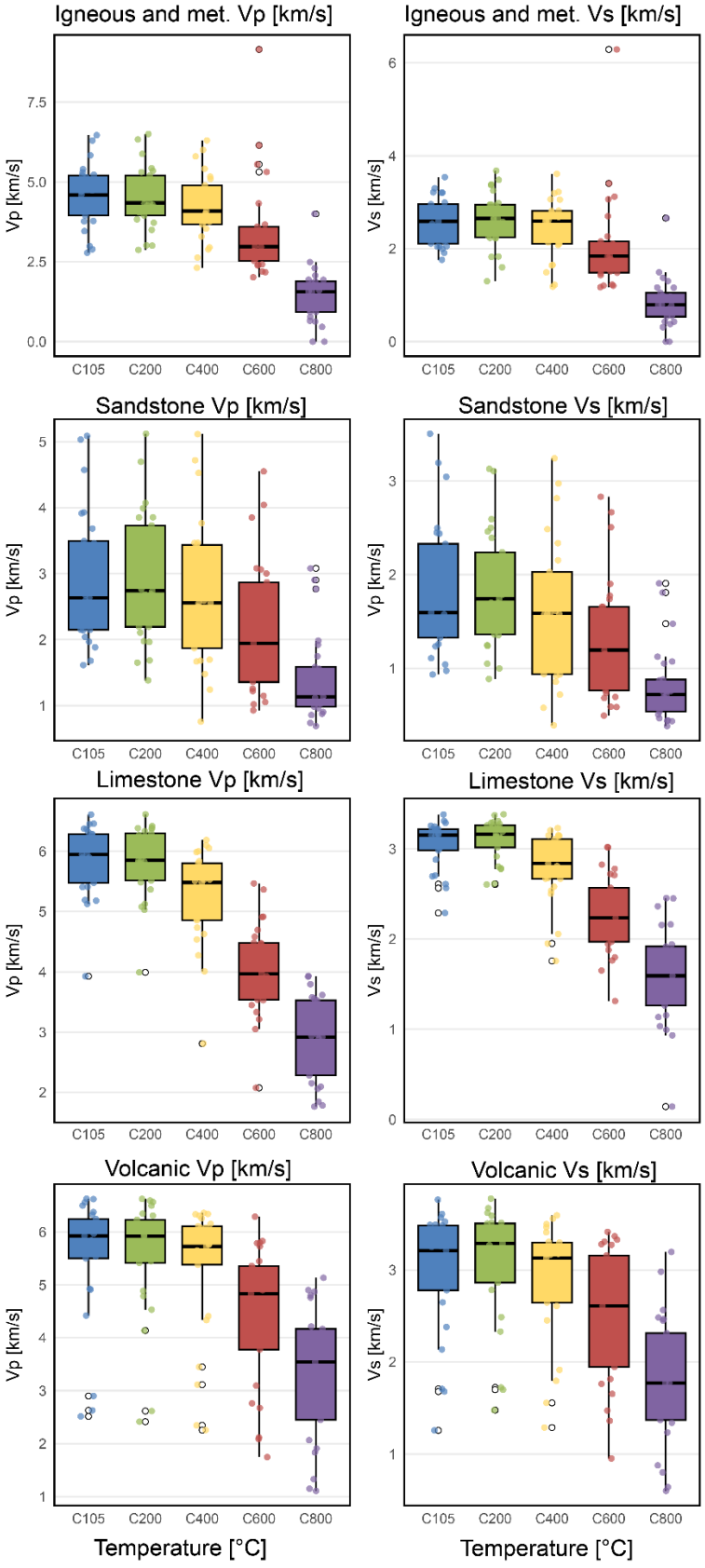

Fig. 4 Vp and Vs velocities of thermally treated UCS specimens for igneous and metamorphic, sandstone, limestone, and volcanic rocks across five temperature conditions (from 105 °C to 800 °C). Each subplot displays the distribution of velocities, highlighting lithological contrasts in material behaviour. Median values, interquartile ranges, and outliers illustrate the progressive degradation of wave propagation with increasing temperature.

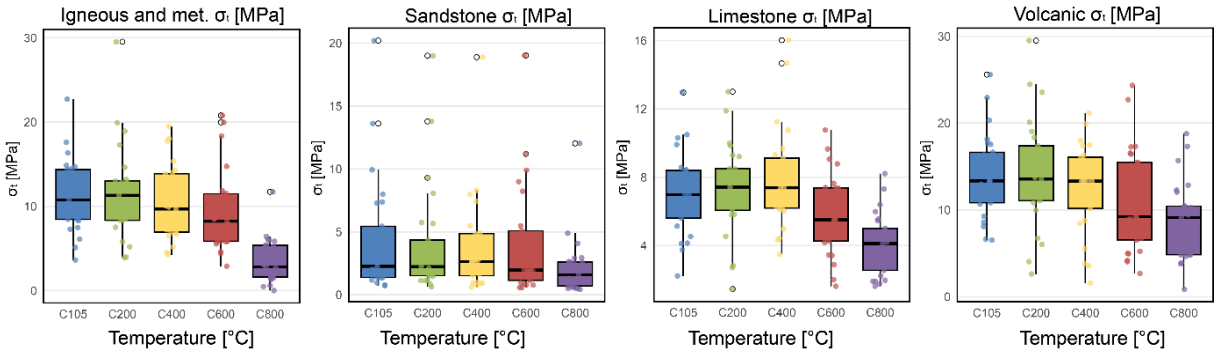

Fig. 5 Changes in tensile strength of thermally treated igneous and metamorphic, sandstone, limestone and volcanic BTS specimens.

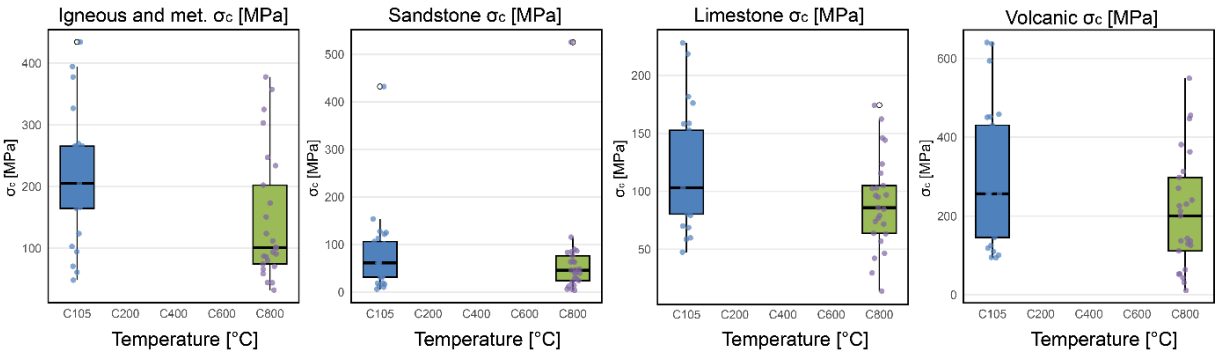

Fig. 6 Changes in compressive strength of thermally treated igneous and metamorphic, sandstone, limestone, and volcanic UCS specimens.

slightly reduced at 200 °C, and decreasing progressively around 400 °C and 600 °C to a more pronounced decrease at 800 °C.

In sandstones, tensile strength initially averages, with only a minor reduction up to 200 °C. However, between 400 °C and 600 °C, tensile strength declines sharply to 800 °C, reaching approximately 30-40 % of its original value.

Limestone specimens show that tensile strength has a corresponding decrease, starting at 200 °C. At 400 °C, tensile strength averages without clear changes, and by 600 °C, it drops by roughly 20 %. At 800 °C, tensile strength is often reduced by about 40–50 % of its original value. Conversely, in volcanic specimens, tensile strength begins and remains relatively unchanged at 100-200 °C. At 400 °C, the reduction becomes clear. By 600 °C, tensile strength decreases by approximately 25 %, and at 800 °C, it often falls by 40 % of its original value.

3.2.2. UCS SPECIMENS

In igneous and metamorphic rocks, compressive strength decreases markedly between 105 °C and 800 °C. The distributions at 80 °C show substantially lower median values and reduced upper ranges compared to 105 °C, indicating pronounced thermal weakening.

Sandstones exhibit a small reduction in compressive strength from 105 °C to 800 °C. While strength at 105 °C spans a relatively wide range with higher medians, and values at 800 °C cluster at lower levels, suggesting strong sensitivity to high-temperature exposure.

Limestones show a decrease in compressive strength between 105 °C and 800 °C. The 800 °C boxplots display both lower medians and narrower ranges, suggesting that most samples undergo significant strength loss at elevated temperature.

Volcanic rocks present a more variable response, but still with an overall decline in compressive strength from 105 °C to 800 °C. Some specimens retain comparatively higher strength at 800 °C, whereas others drop to low values, highlighting heterogeneous thermal behaviour within this lithology.

3.2.3. FT SPECIMENS

Igneous and metamorphic rocks show a clear reduction in K_{IC} with increasing temperature. Values at 105 °C are the highest and display moderate variability, while at 350 °C, no decrease is observed. By 600 °C, K_{IC} drops sharply, with most samples reaching the lowest range of the dataset, reflecting substantial thermal degradation.

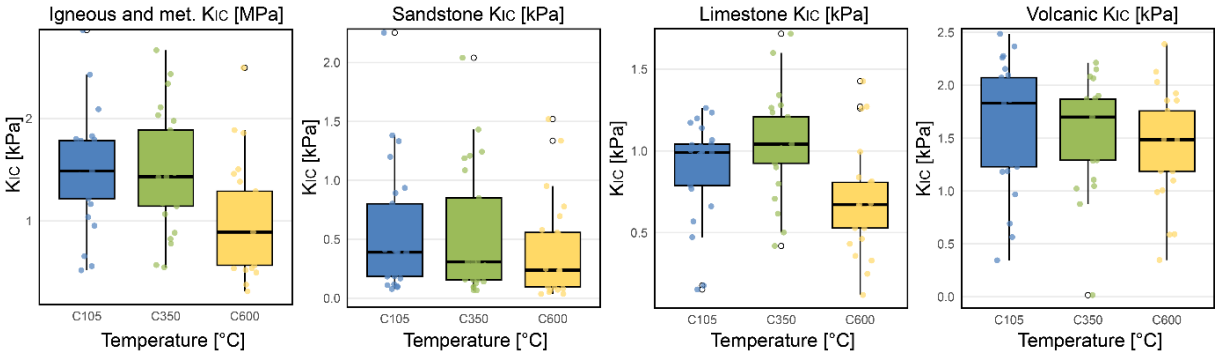

Fig. 7 Changes in K_{IC} of thermally treated igneous and metamorphic, sandstone, limestone, and volcanic FT specimens.

Sandstones exhibit a progressive decline in K_{IC} across the temperature steps. K_{IC} at 105 °C has high dispersion, but a small reduction appears already at 350 °C. At 600 °C, median K_{IC} falls to low values, with a narrower distribution indicating that most samples converge toward a similarly weakened condition.

Limestones show an unusual behaviour in KIC values between 105 °C and 350 °C. The reduction becomes more pronounced at 600 °C, where KIC values drop significantly, and variability decreases.

Volcanic rocks display the most variable response, where KIC at 105 °C spans a wide range, 350 °C, decreases but retains considerable scatter, and 600 °C, most samples show a strong reduction. However, a few retain comparatively higher FT, highlighting the lithological diversity.

4. DISCUSSIONS

It has to be pointed out that the presumed mineralogical changes of rock under thermal treatment discussed in the following paragraphs are extracted from the literature, as the nature of the nation-wide study did not allow to analyse large number of thin-sections (1000 specimens from 100 sites).

4.1. BTS SPECIMENS

For igneous and metamorphic rocks, the strong reduction in both Vp and Vs amplitudes with temperature is most probably mainly due to the formation and propagation of thermal microcracks along grain boundaries and cleavage planes, as also shown by the decay in tensile strength (Figs. 5, 8). Above 400 °C, differences in thermal expansion coefficients between mineral phases (e.g., quartz, feldspar, micas) become critical, producing intergranular fractures that disrupt the continuity of the elastic wave path. Several studies of granite show extensive microcracking during cooling and contraction, leading to reduced wave velocities, while heating itself causes fewer new cracks but still degrades elasticity (Guo et al., 2023). Above 600 °C, the alpha-beta quartz transition (Tomás et al., 2021) is most probably responsible for the sudden drop in Vp and Vs velocities. The Vp velocity decreases with temperature following the quadratic function (R^2 = 0.973). At 100 °C, values remain above 4.0 km/s, while by 800 °C, velocities fall below 2 km/s, indicating a significant thermal sensitivity. Vs velocities show a similar trend (R^2 = 0.982), decreasing from above 2.2 km/s at 100 °C to below 1 km/s at 800 °C. Tensile strength declined from ~10 MPa at 100 °C to less than 2 MPa at 800 °C. These results confirm the strong degradation of igneous and metamorphic rocks at elevated temperatures, associated with microcracking phenomena.

In sandstones, the moderate decrease in velocities up to 400 °C and the sharper decline thereafter can be possibly linked to the behaviour of quartz grains and the nature of the cementing matrix (Fig. 8). However, in recent study of Filippi et al. (2026) from wildfire affected sandstone area in the Czech Republic, only minor mineralogical changes were observed for temperatures from 250 to 310 °C. At lower temperatures, expansion of the grains and the cement is relatively uniform, so damage is limited. Beyond 400 °C, differential expansion between quartz grains and cement, along with the breakdown of clay minerals or iron oxides in the cement, can cause progressive loss of grain-to-grain contact (Hajpál and Török, 2004). The slightly higher resistance of Vs at moderate heating suggests that shear wave paths initially remain less affected by intergranular changes, but high-temperature cracking disrupts both Vp and Vs propagation similarly. Particularly, our sandstone specimens show moderate reductions in Vp velocities up to ~400 °C, followed by accelerated declines beyond this temperature. Vp velocity decreases according to a quadratic function (R^2 = 0.991), similarly to the crystalline rocks. The initial velocity of ~2.8 km/s at 100 °C decreases steadily to ~1.5 km/s at 800 °C. Similar behaviour was also observed in the study of Yang et al. (2022). The Vs velocity trend (R^2 = 0.967) indicates a reduction from ~1.9 km/s to below 1.0 km/s over the same temperature range. Tensile strength shows larger scatter (Fig. 5), dropping from ~4 MPa at 100 °C to about 1 MPa at 800 °C. This demonstrates that sandstones lose both stiffness and strength more gradually than crystalline rocks but still undergo notable deterioration.

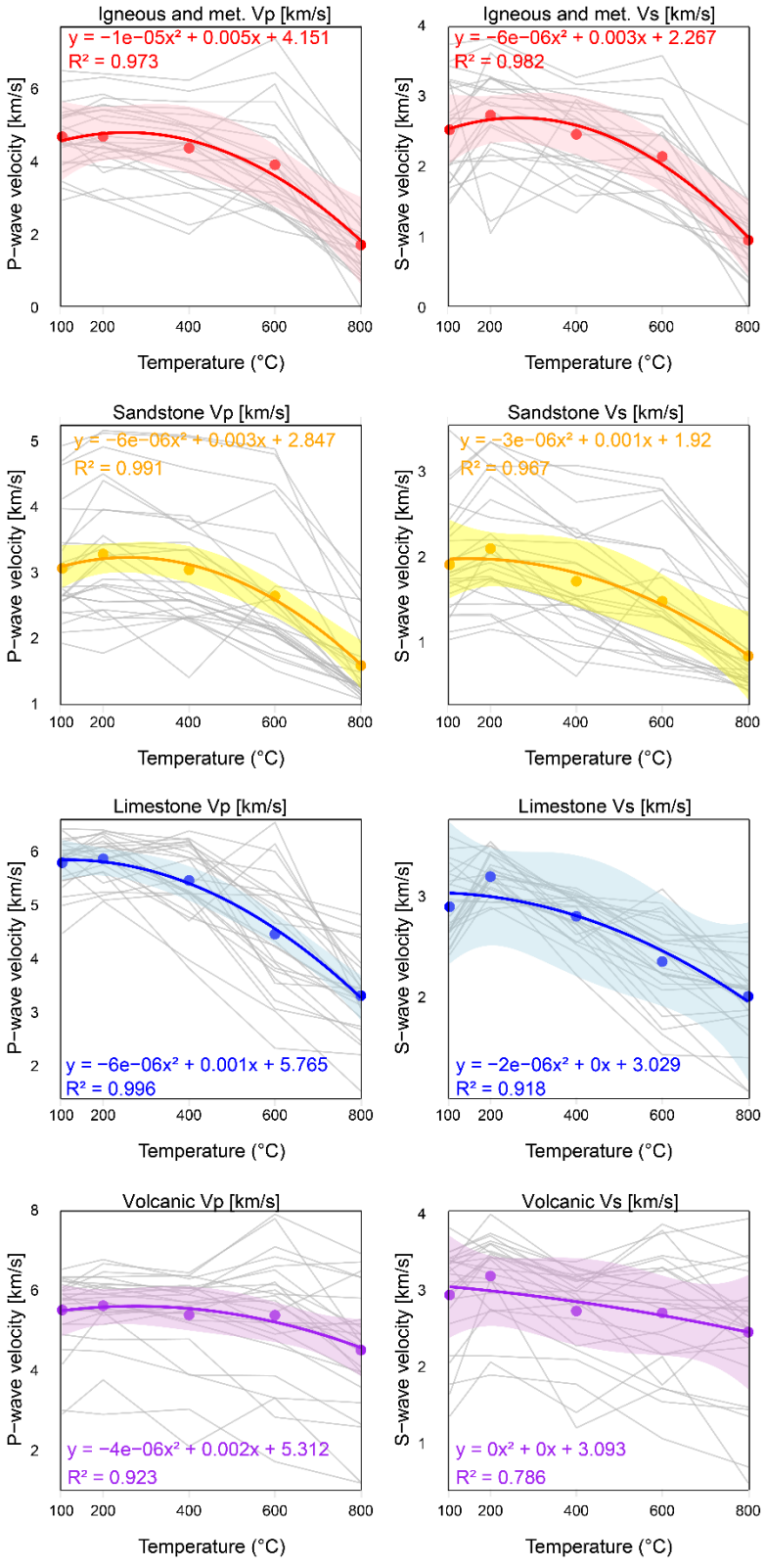

Fig. 8 Vp and Vs velocities of thermally treated BTS specimens. The rock's behaviour has been approximated by a quadratic function. The results showed outstanding values in R^2.

Limestones show a steadier decline, with Vp amplitudes being less affected than in crystalline rocks or sandstones (Fig. 8). This behaviour might be linked to the thermal expansion of calcite, which is more uniform than that of crystalline rocks. However, above 400 °C, incipient calcite decomposition and pore enlargement from microcracking lead to a more pronounced decrease in Vs velocities. The greater variability in Vs is likely due to the sensitivity of shear wave propagation to small-scale anisotropy caused by preferential crack orientation. Calcite recrystallisation at high temperatures may locally reinforce some wave paths, accounting for the smaller Vp losses in some specimens. Beyond ~400 °C–500 °C, calcite and dolomite phases undergo decomposition, causing microcracking, increased porosity, and loss of elastic properties (Vagnon et al., 2023; Zhang et al., 2024). The Vp velocity reduction (R^2 = 0.996), with initial values around 5.7 km/s at 100 °C, declines to ~3.0 km/s at 800 °C. Vs velocities (R^2 = 0.918) showed a less pronounced reduction from ~3.0 km/s to ~2.0 km/s (Fig. 8). While tensile strength decreases, with values dropping from ~6 MPa to below 2 MPa at 800 °C (Fig. 5). The higher initial velocities and strength of limestones confirm their denser and less porous fabric, although they still exhibit pronounced thermal weakening. Tensile strength showed a high variability, especially around 400 °C.

Volcanic rocks display a wide range of responses due to their heterogeneous mineralogy, textures, and porosity (Fig. 8). The presence of glassy phases and phenocrysts means that thermal damage is unevenly distributed, with some specimens showing early crack development and others remaining relatively intact up to high temperatures. Expansion mismatch between crystalline phenocrysts and the glassy matrix often causes localised damage that disrupts wave paths irregularly. Volcanic rocks heated and cooled show that most thermal damage and cracking occur during cooling, when tensile stresses propagate microcracks more widely than during heating. These thermal contraction cracks degrade elastic wave velocities and mechanical integrity (Browning et al., 2016; Ahmed et al., 2022). Vp velocity (R^2 = 0.923), decreased from ~5.3 km/s at 100 °C to below 3.0 km/s at 800 °C. Vs velocity shows limited sensitivity (R^2 = 0.786), with values remaining ~3 km/s across the entire temperature range. Tensile strength declines sharply (Fig. 5), from ~14 MPa at 100 °C to ~5 MPa at 800° C. Compared to the other lithologies, volcanic rocks retain Vs velocities but exhibit a strong loss of tensile resistance, likely linked to heterogeneous textures and pore structures.

4.2. UCS SPECIMENS

UCS specimens have also been used to represent larger sample heights and to compute uniaxial strength. In general, the results seem in accordance with the BTS samples, although differences in velocities are present. Temperature-dependent reductions in seismic velocities and compressive strength have been documented and are commonly attributed to thermally induced microcracking and differential thermal expansion within the rock matrix (Janssen et al., 2021; Pimienta et al., 2019; Keshavarz et al., 2010; Kern et al., 2011). In Figure 9, the Vp for igneous and metamorphic rocks decreases with temperature following a quadratic trend (R^2 = 0.989), starting at approximately 4.1 km/s at 100 °C and dropping below 2.5 km/s by 800 °C. The Vs velocity also follows a quadratic decline (R^2 = 0.979), beginning around 2.3 km/s and falling to just above 1.0 km/s at the highest temperature. The uniaxial compressive strength showed, instead, a marked reduction between the two measured points, with values decreasing from roughly 10 MPa at 100 °C to below 2 MPa at 800 °C (Fig. 6). All sources agree that high temperatures or thermal cycling led to the formation and growth of microcracks because of different mineral thermal expansion rates. This causes reductions in rock elastic moduli and compressive strength. Additionally, factors such as fluids (water) and cooling regimes (timing, temperature) influence mechanical changes, including crack opening or closing (Popoola et al., 2025; Zhang et al., 2022, Yu et al., 2021, Gao et al., 2021)

Sandstone plots show a quadratic decrease in Vp velocity (R^2 = 0.998), beginning at about 2.9 km/s at 100 °C and declining to near 1.5 km/s at 800 °C. The Vs velocity remains nearly linear (R^2 = 0.998), starting at approximately 1.85 km/s and ending below 1.0 km/s. The UCS data points indicate a drop from around 4 MPa at 100 °C to approximately 1 MPa at 800 °C, with visible error bars suggesting variability. The wave velocity regressions are tightly fitted, while the strength data show more scatter. Similar behaviour has been reported for sandstone and quartz-bearing rocks subjected to elevated temperatures, where differential thermal expansion among mineral grains promotes intergranular microcracking and crack opening, leading to progressive reductions in P- and S-wave velocities as well as in compressive strength. (Lokajíček et al., 2026; Pimienta et al., 2019), often resulting in tensile failure at elevated temperatures (Yang et al., 2026).

Limestones exhibits high initial Vp velocities (~6.0 km/s at 100 °C), which decrease quadratically (R^2 = 0.995) to about 3.5 km/s at 800 °C. Vs velocities follow a similar pattern (R^2 = 0.996), starting near 3.1 km/s and reducing to around 2.0 km/s. UCS values drop from roughly 6 MPa to below 2 MPa between the two temperature points. The plots show consistent trends across all three properties, with relatively tight regression fits for both wave velocities and moderate variability in strength. In carbonate rocks, such reductions are commonly linked to thermally induced microfracturing and the decomposition of carbonate minerals at elevated temperatures, which significantly affect both elastic wave propagation and mechanical strength (Ferrero and Marini, 2001).

Volcanic rocks display a quadratic decrease in Vp velocity (R^2 = 0.999), from about 5.3 km/s at

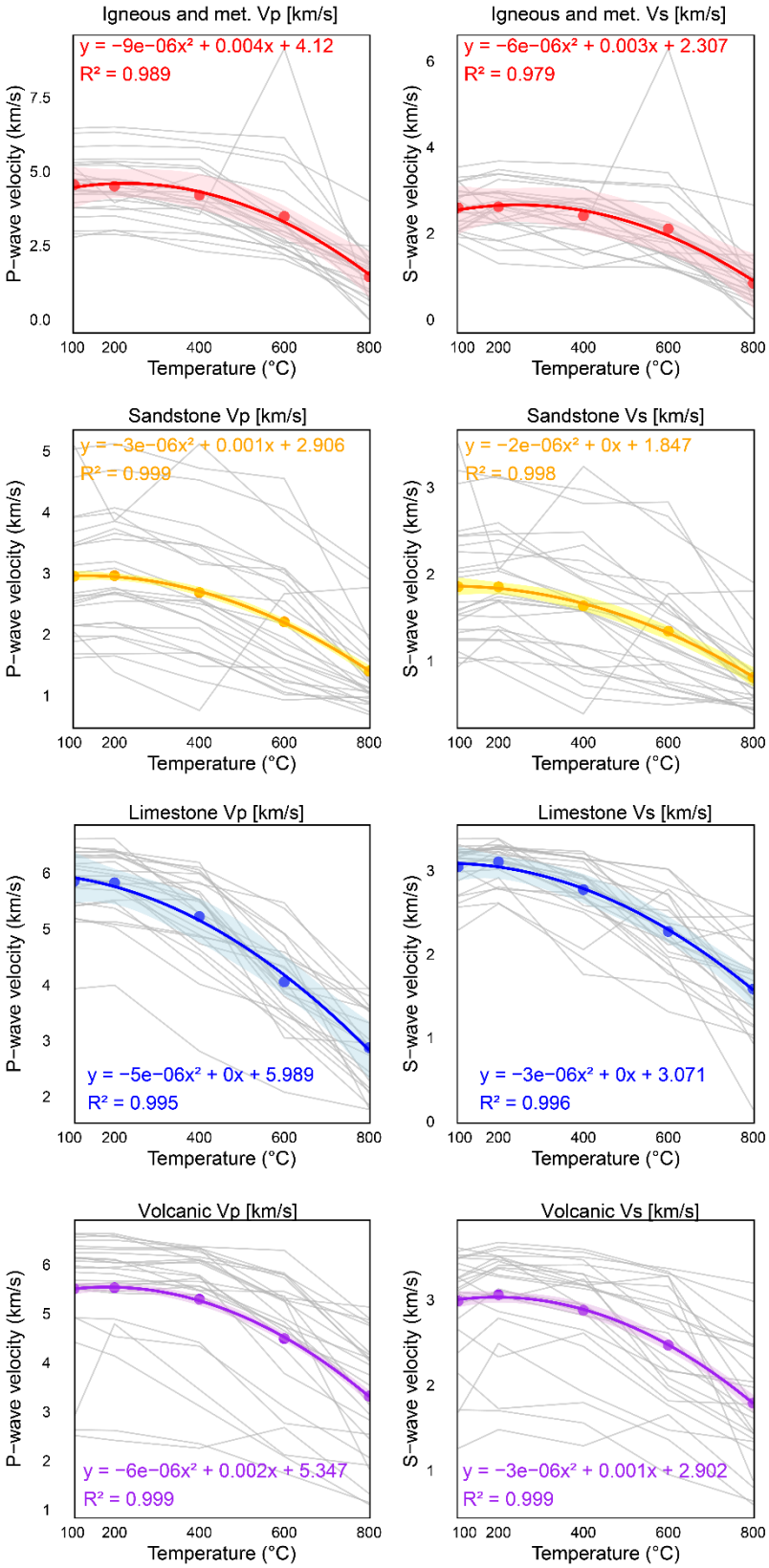

Fig. 9 Vp and Vs velocities of thermally treated rocks. The rock's behaviour has been approximated by a quadratic function. The results showed outstanding values in R^2.

100 °C to below 3.0 km/s at 800 °C. Vs velocity also declines (R^2 = 0.999), starting at approximately 2.9 km/s and ending near 1.5 km/s. The σ_c values show a sharp reduction, from around 14 MPa at 100 °C to about 5 MPa at 800 °C, with error bars indicating some variability. Both destructive and non-destructive methods exhibit clear temperature-dependent declines, suggesting the volcanic rocks as a possible target of fire degradation. Similar temperature-induced degradation has been reported for volcanic rocks, where thermal cracking and pore expansion contribute to reductions in elastic wave velocities and compressive strength (Heap et al., 2014).

5. SUMMARY AND CONCLUSIONS

Igneous and metamorphic, and volcanic rocks exhibited rapid P and S wave velocity loss with increasing temperature, most probably due to the development of thermal microcracks driven by mineral expansion mismatches and cooling-induced tensile stresses. Sandstones showed a more gradual reduction, reflecting the role of cement mineralogy and grain-boundary structure in moderating thermal damage. Limestones instead were particularly sensitive beyond 400 °C, where thermal decomposition of calcite and dolomite probably accelerated porosity growth and mechanical weakening. Interestingly, initial velocity increases observed in some samples at 200 °C may suggest transient strengthening mechanisms such as microcrack closure. However, these effects were outweighed by progressive degradation at higher temperatures and warrant further investigation. Additionally, it was observed that tensile strength and K_{IC} in igneous and metamorphic rocks and limestones were non-linear, while sandstones and volcanic rocks showed a marked linear behaviour.

We are aware of missing thin-section analyses, which might decipher the mineralogical changes. However, the purpose of the study was to assess the mechanical changes in a broad, quantitative way, by collecting samples from 100 sites across the country and 1000 specimens analysed. Selected samples will, however, be subject to more detailed analysis, including mineralogical composition changes and mercury porosimetry in the near future.

Overall, the large sampling and variety of tests and destructive and non-destructive techniques helped in better defining the possible behaviour of the four lithotypes. In this perspective, our work, incorporating lithology-specific thermal response data and functions, might be beneficial for estimating material behaviour, and it will improve predictions of high temperature rock degradation and thermal fatigue and support targeted risk mitigation in landscapes experiencing more frequent and severe fires under a warming climate in Central Europe, and particularly in the Czech Republic.

DECLARATION OF GENERATIVE AI AND AI-ASSISTED TECHNOLOGIES IN THE WRITING PROCESS

No generative AI or AI-assisted technologies were used in the preparation of this manuscript, except for limited language editing.

AUTHOR CONTRIBUTIONS

G.R. Data curation, Methodology, Formal analysis, Writing; M.L. Conceptualisation, Methodology, Visualisation, Writing – original draft; O.R. Data curation, Methodology; X.-X.N. Formal analysis, Investigation; A.P. Formal analysis, Investigation; J.B. Conceptualisation, Funding acquisition, Methodology, Project administration, Writing - original draft.

FUNDING

This research was performed in the framework of the long-term conceptual development research organisation RVO: 67985891. This research was supported by the Technology Agency of the Czech Republic within the Prostředí pro život Programme project n. SS07010216.

REFERENCES

Aboayanah, K.R., Ossetchkina, E., Abdelaziz, A., Sun, L., Peterson, K. and Grasselli, G.: 2024, Effect of thermal pre-treatment on thermal gradient response of granitic rocks: Insights from optical microscopy and digital image correlation. Rock Mech. Rock Eng, 57, 12, 10805-10830. DOI: 10.1007/s00603-024-04125-9

Ahmed, H.M., Hefni, M.A., Ahmed, H.A., Adewuyi, S.O., Hassani, F., Sasmito, A.P. and Hassan, G.S.: 2022, Effect of elevated temperature on rhyolitic rocks' properties. Materials, 15, 9, 3204. DOI: 10.3390/ma15093204

Bieniawski, Z.T. and Bernede, M.J.: 1979, Suggested methods for determining the uniaxial compressive strength and deformability of rock materials: Part 1. Suggested method for determining deformability of rock materials in uniaxial compression. In: Int. J. Rock Mech. Min. Sci. Geomech. Abstr., 16, 2, 138–140. DOI: 10.1016/0148-9062(79)91451-7

Browning, J., Meredith, P. and Gudmundsson, A.: 2016, Cooling-dominated cracking in thermally stressed volcanic rocks. Geophys. Res. Lett., 43, 16, 8417–8425. DOI: 10.1002/2016GL070532

Buckman, S., Morris, R.H. and Bourman, R.P.: 2021, Fire-induced rock spalling as a mechanism of weathering responsible for flared slope and inselberg development. Nat. Commun., 12, 1, 2150. DOI: 10.1038/s41467-021-22451-2

Chlupáč, I., Brzobohatý, R., Kovanda, J. and Stráník, Z.: 2002, Geological History of the Czech Republic. Academia, 436 pp., (in Czech).

Dally, J.W.: 2008, 11. Statistical analysis of experimental data. In: Sharpe, W.N. (Ed.), Springer Handbook of Experimental Solid Mechanics. Springer, New York, USA, 259–280. DOI: 10.1007/978-0-387-30877-7_11

Dorn, R.I.: 2003, Boulder weathering and erosion associated with a wildfire, Sierra Ancha Mountains, Arizona. Geomorphology, 55, 1-4, 155–171. DOI: 10.1016/S0169-555X(03)00138-7

Dupuy, J., Fargeon, H., Martin-StPaul, N., Pimont, F., Ruffault, J., Guijarro, M., Hernando, C., Madrigal, J. and Fernandes, P.: 2020, Climate change impact on future wildfire danger and activity in southern Europe: a review. Ann. For. Sci., 77, 2, 35. DOI: 10.1007/s13595-020-00933-5

Ferrero, A. and Marini, P.:2001, Experimental studies on the mechanical behaviour of two thermal cracked marbles. Rock Mech. Rock Eng., 34, 57–66. DOI: 10.1007/s006030170026

Filippi, M., Adamovič, J., Slavík, M., Mikysek, P., Weiss, T., Mareš, J., Bruthans, J. and Rohovec, J.: 2026, Effects of wildfire on sandstone outcrops and environmental consequences, Bohemian Switzerland NP, Czech Republic. CATENA, 264, 109831. DOI: 10.1016/j.catena.2026.109831

Gao, Y., Wang, Y., Lu, T., Li, L., Wu, J. and Zhang, Z.: 2021, An experimental study on the mechanical properties of high-temperature granite under natural cooling and water cooling. Adv. Mat. Sci. Eng., 9018462, 11 pp. DOI: 10.1155/2021/9018462

Gill, D.E., Corthésy, R. and Leite, M.H.: 2005, Determining the minimal number of specimens for laboratory testing of rock properties. Eng. Geol., 78, 1-2, 29–51. DOI: 10.1016/j.enggeo.2004.10.005

Goudie, A.S.: 1999, Experimental salt weathering of limestones in relation to rock properties. Earth Surf. Processes Landforms, 24, 8, 715–724. DOI: 10.1002/(SICI)1096-9837(199908)24:8<715

Goudie, A.S., Allison, R.J. and McLaren, S.J.: 1992, The relations between modulus of elasticity and temperature in the context of the experimental simulation of rock weathering by fire. Earth Surf. Processes Landforms, 17, 6, 605–615. DOI: 10.1002/esp.3290170606

Guo, P., Zhang, P., Bu, M., Wang, J., Zheng, X. and He, M.: 2023, Microcracking behavior and damage mechanism of granite subjected to high temperature based on CT-GBM numerical simulation. Comput. Geotech., 159, 105385. DOI: 10.1016/j.compgeo.2023.105385

Hajpál, M. and Török, Á.: 2004, Mineralogical and colour changes of quartz sandstones by heat. Env. Geol., 46, 311–322. DOI: 10.1007/s00254-004-1034-z

Heap, M.J., Lavallée, Y., Petrakova, L., Baud, P., Reuschlé, T., Varley, N.R. and Dingwell, D.B.: 2014, Microstructural controls on the physical and mechanical properties of edifice-forming andesites at Volcán de Colima, Mexico. J. Geophys. Res. Solid Earth, 119, 2925–2963. DOI: 10.1002/2013JB010521.

Hillayová, M.K., Holécy, J., Korísteková, K., Bakšová, M., Ostrihoň, M. and Škvarenina, J.: 2023, Ongoing climatic change increases the risk of wildfires. Case study: Carpathian spruce forests. J. Environ. Manage., 337, 117620. DOI: 10.1016/j.jenvman.2023.117620

Hlásný, T., Mátyás, C., Seidl, R., Kulla, L., Merganičová, K., Trombik, J., Dobor, L., Barcza, Z. and Konôpka, B.: 2014, Climate change increases the drought risk in Central European forests: What are the options for adaptation? Cent. Eur. For. J., 60, 1, 5–18. DOI: 10.2478/forj-2014-0001

Hruška, J., Balek, J., Beranová, J., Bláhová, M., Bobek, P., Cienciala, E., Homolová, L., Kudláčková, L., Krajhanzl, J. and Možný, M.: 2022, What factors influenced the outbreak and spread of the fire in the Bohemian Switzerland National Park. MŽP. Available at: https://mzp.gov.cz/system/files/2024-10/OZUOPK-studie_pozar_NPCS-20230105.pdf.pdf , (in Czech).

ISRM: 1978, Suggested methods for determining tensile strength of rock materials Part 2: Suggested method for determining indirect tensile strength by the Brazil Test. Int. J. Rock Mech. Min. Sci., 15, 3, 99–103. DOI: 10.1016/0148-9062(78)90003-7

Janssen, M.T.G., Barnhoorn, A., Draganov, D., Wolf, K.-H. and Durucan, S.: 2021, Seismic velocity characterisation of geothermal reservoir rocks for CO2 storage performance assessment. Appl. Sci., 11, 8, 3641. DOI: 10.3390/app11083641

Kern, H.: 2011, Measuring and modeling of P- and S-wave velocities on crustal rocks: A key for the interpretation of seismic reflection and refraction data. Int. J. Geophys., 530728, 9 pp. DOI: 10.1155/2011/530728

Keshavarz, M., Pellet, F.L. and Loret, B.: 2010. Damage and changes in mechanical properties of a gabbro thermally loaded up to 1,000°C. Pure Appl. Geophys., 167, 1511–1523. DOI: 10.1007/s00024-010-0130-0

Kompaníková, Z., Gomez-Heras, M., Michňová, J., Durmeková, T. and Vlčko, J.: 2014, Sandstone alterations triggered by fire-related temperatures. Environ. Earth Sci., 72, 2569–2581. DOI: 10.1007/s12665-014-3164-2

Kudláčková, L., Poděbradská, M., Bláhová, M., Cienciala, E., Beranová, J., McHugh, C., Finney, M., Novotný, J., Zahradníček, P., Štěpánek, P., Linda, R., Pikl, M., Vébrová, D., Možný, M., Surový, P., Žalud, Z. and Trnka, M.: 2024, Using FlamMap to assess wildfire behavior in Bohemian Switzerland National Park. Nat. Hazard., 120, 4, 3943–3977. DOI: 10.1007/s11069-023-06361-8

Kuruppu, M.D., Obara, Y., Ayatollahi, M.R., Chong, K.P. and Funatsu, T.: 2014, ISRM-suggested method for determining the mode I static fracture toughness using semi-circular bend specimen. Rock Mech. Rock Eng., 47, 1, 267–274. DOI: 10.1007/s00603-013-0422-7

Lainas, S., Depountis, N. and Sabatakakis, N.: 2021, Preliminary forecasting of rainfall-induced shallow landslides in the wildfire burned areas of western Greece. Land, 10, 8, 877. DOI: 10.3390/land10080877

Loche, M., Usmanova, D., Racek, O., Avcıoğlu, A., Görüm, T., Adamovič, J. and Blahůt, J.: 2026, Response of rock material properties of quartzose sandstones to wildfire: a case study from Bohemian Switzerland National Park, Czechia. Bull. Eng. Geol. Env., 85, 1, 76. DOI: 10.1007/s10064-025-04748-4

Lokajíček, T., Přikryl, R., Racek, M., Řimnáčová, D., Natherová, V., Petružálek, M., Svitek, T. and Aminzadeh, A.: 2026, Influence of thermal loading on microcrack evolution and elastic anisotropy in Westerly granite. Rock Mech. Rock Eng., 59, 2667–2691. DOI: 10.1007/s00603-025-04939-1

Matula, M. and Pašek, J.: 1986, Regional Engineering Geology of CSSR. ALFA, SNTL, 296 pp., (in Czech).

McCaffrey, S.: 2004, Thinking of wildfire as a natural hazard. Soc. Nat. Resour., 17, 6, 509–516. DOI: 10.1080/08941920490452445

Moreira, F., Viedma, O., Arianoutsou, M., Curt, T., Koutsias, N., Rigolot, E., Barbati, A., Corona, P., Vaz, P., Xanthopoulos, G., Mouillot, F. and Bilgili, E.: 2011, Landscape – wildfire interactions in southern Europe: Implications for landscape management. J. Env. Manage., 92, 10, 2389–2402. DOI: 10.1016/j.jenvman.2011.06.028

Nasseri, M.H.B., Schubnel, A. and Young, R.P.: 2007, Coupled evolutions of fracture toughness and elastic wave velocities at high crack density in thermally

treated Westerly granite. Int. J. Rock Mech. Min. Sci., 44, 4, 601–616. DOI: 10.1016/j.ijrmms.2006.09.008

Nyman, P., Rutherfurd, I.D., Lane, P.N.J. and Sheridan, G.J.: 2019, Debris flows in southeast Australia linked to drought, wildfire, and the El Niño–Southern Oscillation. Geology, 47, 5, 491–494. DOI: 10.1130/G45939.1

Packulak, T.R.M., Day, J.J., McDonald, M.R., Jacksteit, A.C. and Diederichs, M.S.: 2025, Measurement of true tensile strength from Brazilian tensile strength laboratory tests. Can. Geotech. J., 62, 1–14. DOI: 10.1139/cgj-2023-0204

Pimienta, L., Orellana, L.F. and Violay, M.: 2019, Variations in elastic and electrical properties of crustal rocks with varying degree of microfracturation. J. Geophys. Res., Solid Earth, 124, 6376–6396. DOI: 10.1029/2019JB017339

Popoola, A.K., Chapman, S., Ògúnsàmì, A., Fortin, J. and Grasselli, G.: 2025, Impact of thermally induced cracks on elastic modulus dispersion and attenuation in fluid-saturated granite. J. Geoph. Res. Solid Earth, 130, e2024JB030977. DOI: 10.1029/2024JB030977

Ram, B.K., Das, R. and Mishra, D.A.: 2025, Thermal treatment induced damage mechanism of rock materials and its influence on the physico-mechanical properties - a review. Environ. Earth Sci., 84, 12, 334. DOI: 10.1007/s12665-025-12300-6

Řimnáčová, D., Natherová, V., Lokajíček, T., Petružálek, M., Aminzadeh, A., Racek, M. and Přikryl, R.: 2024, Thermally induced degradation of Westerly granite microstructure documented by dynamic elastic properties and pore space and damage characteristics. Bull. Eng. Geol.Environ., 83, 12, 518. DOI: 10.1007/s10064-024-04011-2

Ruffault, J., Curt, T., Moron, V., Trigo, R.M., Mouillot, F., Koutsias, N., Pimont, F., Martin-StPaul, N., Barbero, R., Dupuy, J.-L., Russo, A. and Belhadj-Khedher, C.: 2020, Increased likelihood of heat-induced large wildfires in the Mediterranean Basin. Sci. Rep., 10, 1, 13790. DOI: 10.1038/s41598-020-70069-z

Sarro, R., Pérez-Rey, I., Tomás, R., Alejano, L.R., Hernández-Gutiérrez, L.E. and Mateos, R.M.: 2021, Effects of wildfire on rockfall occurrence: a review through actual cases in Spain. Appl. Sci., 11, 6, 2545. DOI: 10.3390/app11062545

Scaringi, G. and Loche, M.: 2022, A thermo-hydro-mechanical approach to soil slope stability under climate change. Geomorphology, 401, 108108. DOI: 10.1016/j.geomorph.2022.108108

Schelhaas, M.-J., Hengeveld, G., Moriondo, M., Reinds, G.J., Kundzewicz, Z.W., Ter Maat, H. and Bindi, M.: 2010, Assessing risk and adaptation options to fires and windstorms in European forestry. Mitigation Adapt. Strategies Global Change, 15, 681–701. DOI: 10.1007/s11027-010-9243-0

Schön, J.H. (Ed.): 2015, Physical properties of rocks: Fundamentals and principles of petrophysics. Dev. Pet. Sci., 65, Elsevier, 497 pp.

Shtober-Zisu, N. and Wittenberg, L.: 2021a, Long-term effects of wildfire on rock weathering and soil stoniness in the Mediterranean landscapes. Sci. Total Environ., 762, 143125. DOI: 10.1016/j.scitotenv.2020.143125

Shtober-Zisu, N. and Wittenberg, L.: 2021b, Wildfires as a weathering agent of carbonate rocks. Minerals, 11, 10, 1091. DOI: 10.3390/min11101091

Svoboda, J. et al.: 1966, Regional Geology of Czechoslovakia, Part I The Bohemian Massif. Geological Survey of Czechoslovakia, 668 pp.

Tomás, R., Cano, M., Pulgarín, L.F., Brotóns, V., Benavente, D., Miranda, T. and Vasconcelos, G.: 2021, Thermal effect of high temperatures on the physical and mechanical properties of a granite used in UNESCO World Heritage sites in north Portugal. J. Build. Eng., 43, 102823. DOI: 10.1016/j.jobe.2021.102823

Trnka, M., Možný, M., Jurečka, F., Balek, J., Semerádová, D., Hlavinka, P., Štěpánek, P., Farda, A., Skalák, P. and Cienciala, E.: 2021, Observed and estimated consequences of climate change for the fire weather regime in the moist-temperate climate of the Czech Republic. Agric. For. Meteorol., 310, 108583. DOI: 10.1016/j.agrformet.2021.108583

Ulusay, R. and Hudson, J.: 2007, The Blue Book: The complete ISRM suggested methods for rock characterization, testing and monitoring: 1974-2006 https://isrm.net/page/show/935 Accessed 15 Jan 2023.

Vagnon, F., Vinciguerra, S.C., Comina, C., Colombero, C., Ferrero, A.M. and Missagia, R.: 2023, Assessing energy balance via seismic and mechanical observations in high temperature induced crack damage in marbles. Heliyon, 9, 9, e19184. DOI: 10.1016/j.heliyon.2023.e19184

Yang, L., Li, J., Yang, D., Chen, W. and Wang, M.: 2026, Mechanisms of thermal strengthening and deterioration in sandstone: Insights from characteristic stress and micro-crack analysis. PLoS One 21, 2, e0342561. DOI: 10.1371/journal.pone.0342561

Yang, Y., Wei, S., Zhang, J., Wu, J and Zhang C.: 2022, Effect study of heat treatment on tensile properties of coarse sandstone. Sci. Rep., 12, 17525. DOI: 10.1038/s41598-022-21164-w

Yeste-Lizán, P., Gomez-Heras, M., García-Rodríguez, M., Pérez-López, R., Carcavilla, L. and Ortega-Becerril, J.A.: 2023, Surface mechanical effects of wildfires on rocks in climbing areas. Fire, 6, 2, 46. DOI: 10.3390/fire6020046

Yıldız, C., Çömert, R., Tanyaş, H., Yılmaz, A., Akbaş, A., Akay, S.S., Yetemen, Ö. and Görüm, T.: 2023, The effect of post-wildfire management practices on vegetation recovery: Insights from the Sapadere fire, Antalya, Türkiye. Front. Earth Sci., 11, 1174155. DOI: 10.3389/feart.2023.1174155

Yu, L., Peng, H., Zhang, Y., and Li, G.: 2021, Mechanical test of granite with multiple water–thermal cycles. Geotherm. Energy, 9, 1. DOI: 10.1186/s40517-021-00186-z

Zhao, Z., Liu, Z., Pu, H. and Li, X.: 2018, Effect of thermal treatment on Brazilian tensile strength of granites with different grain size distributions. Rock Mech. Rock Eng., 51, 4, 1293–1303. DOI: 10.1007/s00603-018-1404-6

Zhang, L., Li, B., Wu, P., Guo, S., Zheng, Y., Li, M. and Zhu, F.: 2024, Experimental study on the dynamic mechanical properties and crashing behaviours of limestone under high temperatures in real-time. Appl. Sci., 14, 22, 10486. DOI: 10.3390/app142210486

Zhang, Y., Zhang, F., Yang, K., and Cai, Z.: 2022, Effects of real-time high temperature and loading rate on deformation and strength behavior of granite. Geofluids, 2022, 6, 1–11. DOI: 10.1155/2022/9426378

SUPPLEMENT

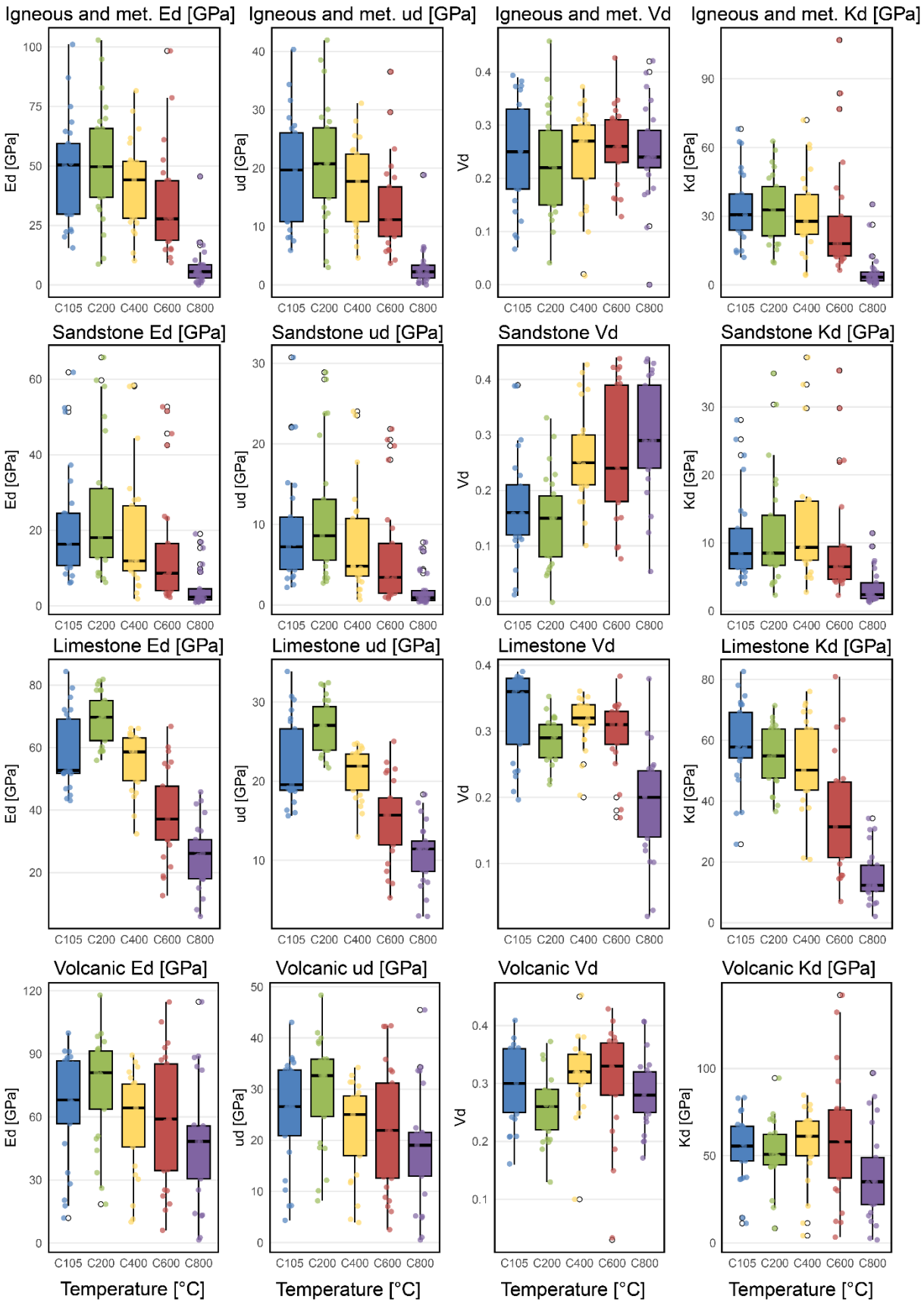

Suppl. Fig. 1 Calculated dynamic elastic moduli for the thermally treated igneous and metamorphic, sandstone, limestone, and volcanic BTS specimens.

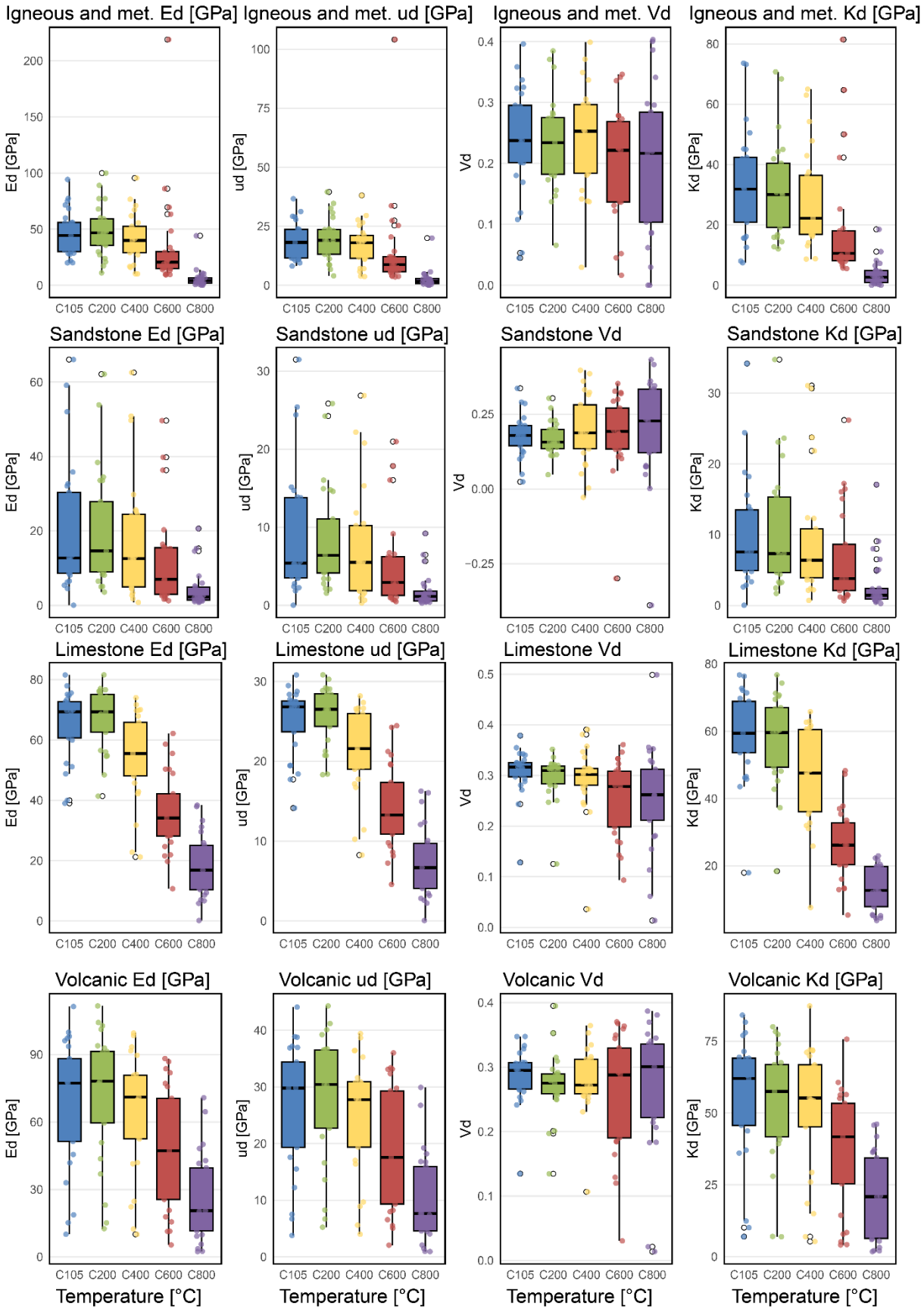

Suppl. Fig. 2 Calculated dynamic elastic moduli for the thermally treated igneous and metamorphic, sandstone, limestone, and volcanic UCS specimens.

Suppl. Table 1 Overview of the locations of the 100 rock samples, including rock type, age, and sampling coordinates.

Sample	Rock Group	Rock Type	Lat.	Lon.	Era	Period
1.	2.	3.	4.	5.	6.	7.
CB10	Igneous and met.	Granite	49.6943	14.4428	Paleozoic	Carboniferous-Permian
CB13	Igneous and met.	Gneiss	49.7004	14.7174	Proterozoic–Paleozoic	Neoproterozoic–Lower Paleozoic
CB2	Igneous and met.	Gabbro	49.9112	14.6601	Paleozoic	Carboniferous-Permian
CB3	Igneous and met.	Gabbro	49.9113	14.6585	Paleozoic	Carboniferous-Permian
CB5	Igneous and met.	Granite	49.9424	14.7948	Paleozoic	Carboniferous-Permian
EB1	Igneous and met.	Phyllite	50.3776	16.1887	Proterozoic–Paleozoic	Neoproterozoic–Lower Paleozoic
EB2	Igneous and met.	Paragneiss	49.7497	15.0830	Proterozoic–Paleozoic	Neoproterozoic–Lower Paleozoic
EB3	Igneous and met.	Granodiorite	49.8814	14.7277	Paleozoic	Carboniferous-Permian
G4	Igneous and met.	Granodiorite	49.8718	14.5328	Paleozoic	Carboniferous-Permian
G5	Igneous and met.	Granodiorite	49.8715	14.5320	Paleozoic	Carboniferous-Permian
NB1	Igneous and met.	Granite	50.7270	15.1583	Paleozoic	Carboniferous
NB14	Igneous and met.	Gneiss	50.5513	13.4998	Paleozoic	Lower Paleozoic
NB2	Igneous and met.	Gneiss	50.7462	13.9175	Paleozoic	Lower Paleozoic
NB25	Igneous and met.	Gneiss	50.5447	13.4715	Paleozoic	Carboniferous
NB8	Igneous and met.	Granite	50.5546	15.5575	Paleozoic	Carboniferous
NB9	Igneous and met.	Granite	50.7513	15.5527	Paleozoic	Carboniferous
SB1	Igneous and met.	Granite	49.0946	14.5803	Paleozoic	Carboniferous
SB4	Igneous and met.	Migmatite	49.1438	15.1189	Proterozoic–Paleozoic	Neoproterozoic–Lower Paleozoic
WB17	Igneous and met.	Rhyolite	50.0701	13.6929	Paleozoic	Cambrium–Ordovician
WB19	Igneous and met.	Porphyritic granite	49.9721	13.4160	Proterozoic–Paleozoic	Neoproterozoic–Lower Paleozoic
WB20	Igneous and met.	Phyllite	49.9852	13.2447	Proterozoic	Neoproterozoic
WB21	Igneous and met.	Granite	50.0833	13.4665	Paleozoic	Paleozoic
WB22	Igneous and met.	Phyllite	49.9448	13.0789	Proterozoic	Neoproterozoic
WB33	Igneous and met.	Migmatite	49.4729	12.7278	Proterozoic–Paleozoic	Neoproterozoic–Lower Paleozoic
WB6	Igneous and met.	Granite	50.0831	13.3396	Proterozoic–Paleozoic	Neoproterozoic–Lower Paleozoic
CB22	Limestones	Limestone	49.8961	14.0294	Paleozoic	Devonian
CB23	Limestones	Limestone	49.9077	14.0664	Paleozoic	Devonian
CB24	Limestones	Limestone	49.9010	14.0727	Paleozoic	Devonian
CB25	Limestones	Limestone	49.9472	14.1364	Paleozoic	Devonian

CB27	Limestones	Limestone	49.9606	14.1836	Paleozoic	Devonian
CB30	Limestones	Limestone	49.9754	14.2308	Paleozoic	Devonian
CB32	Limestones	Limestone	50.0030	14.2719	Paleozoic	Devonian
CB33	Limestones	Limestone	50.0010	14.3290	Paleozoic	Devonian
CB35	Limestones	Limestone	49.9338	14.1522	Paleozoic	Devonian
CB36	Limestones	Limestone	49.9691	14.2248	Paleozoic	Silurian
CB37	Limestones	Limestone	49.9390	14.1175	Paleozoic	Devonian
CB41	Limestones	Limestone	49.9723	14.2563	Paleozoic	Devonian
CM10	Limestones	Limestone	49.3561	16.6979	Paleozoic	Devonian
CM12	Limestones	Limestone	49.3355	16.7347	Paleozoic	Devonian
CM13	Limestones	Limestone	49.2924	16.7230	Paleozoic	Devonian
CM14	Limestones	Limestone	49.3055	16.6937	Paleozoic	Devonian
CM15	Limestones	Limestone	49.2553	16.7553	Paleozoic	Devonian
CM16	Limestones	Limestone	49.2656	16.7476	Paleozoic	Devonian
CM5	Limestones	Limestone	49.3496	16.7438	Paleozoic	Carboniferous–Devonian
CM6	Limestones	Limestone	49.3896	16.7661	Paleozoic	Devonian
CM7	Limestones	Limestone	49.3999	16.7671	Paleozoic	Devonian
NB15L	Limestones	Limestone	50.7906	14.8812	Paleozoic	Carboniferous–Devonian
NB44	Limestones	Limestone	50.6940	15.8497	Paleozoic	Silurian–Devonian
SM1	Limestones	Limestone	48.8567	16.6340	Cenozoic	Paleogene
SM3	Limestones	Limestone	48.8097	16.6557	Mesozoic	Jurassic–Cretaceous
CB16	Sandstones	Sandstone	50.5948	14.4949	Mesozoic	Cretaceous
CB6	Sandstones	Sandstone	50.5270	15.0380	Mesozoic	Cretaceous
EB10	Sandstones	Sandstone	50.3880	15.5300	Mesozoic	Cretaceous
EB4	Sandstones	Sandstone	50.4670	15.3026	Mesozoic	Cretaceous
EB5	Sandstones	Sandstone	50.5736	15.9307	Paleozoic	Permian
EB6	Sandstones	Sandstone	50.4619	15.9320	Cenozoic	Paleogene
EB7	Sandstones	Sandstone	50.4471	15.8600	Mesozoic	Cretaceous
EB8	Sandstones	Sandstone	50.3961	15.7699	Mesozoic	Cretaceous
EB9	Sandstones	Sandstone	50.3893	15.5329	Mesozoic	Cretaceous
NB13	Sandstones	Sandstone	50.6292	15.0927	Mesozoic	Cretaceous
NB15	Sandstones	Sandstone	50.2613	14.0131	Paleozoic	Carboniferous
NB16	Sandstones	Sandstone	50.9020	14.4712	Mesozoic	Cretaceous
NB17	Sandstones	Sandstone	50.9195	14.4596	Mesozoic	Cretaceous
NB18	Sandstones	Sandstone	50.8954	14.4564	Mesozoic	Cretaceous
NB20	Sandstones	Sandstone	50.8570	14.4399	Mesozoic	Cretaceous
NB21	Sandstones	Sandstone	50.8388	14.4324	Mesozoic	Cretaceous
NB4	Sandstones	Sandstone	50.4472	15.4836	Paleozoic	Carboniferous
P2	Sandstones	Sandstone	50.5673	16.2679	Mesozoic	Cretaceous
P5	Sandstones	Sandstone	50.8039	14.0516	Mesozoic	Cretaceous
SM4	Sandstones	Sandstone	49.0972	17.3025	Cenozoic	Paleogene
SM6	Sandstones	Sandstone	49.1086	17.3110	Mesozoic–Cenozoic	Cretaceous–Paleogene
SM8	Sandstones	Sandstone	49.1468	17.7380	Cenozoic	Paleogene
SM9	Sandstones	Sandstone	49.2171	18.0475	Cenozoic	Paleogene
WB11	Sandstones	Sandstone	49.7391	13.5483	Paleozoic	Ordovician
WB14	Sandstones	Sandstone	49.7958	13.8746	Paleozoic	Ordovician
CB19	Volcanic	Spilite	50.0029	13.8053	Proterozoic	Neoproterozoic
CB38	Volcanic	Basalt	50.1854	14.0947	Cenozoic	Tertiary (Paleogene-Tertiary)
CB39	Volcanic	Basalt	50.4133	13.8380	Cenozoic	Tertiary (Paleogene-Tertiary)
CB40	Volcanic	Basalt	50.4376	13.7692	Cenozoic	Tertiary (Paleogene-Tertiary)
NB11	Volcanic	Andesite	50.5636	15.3822	Paleozoic	Carboniferous

NB22	Volcanic	Basalt	50.8208	14.4623	Cenozoic	Tertiary (Paleogene-Tertiary)
NB23	Volcanic	Trachybasalt	50.5976	14.2627	Cenozoic	Tertiary (Paleogene-Tertiary)
NB24	Volcanic	Basalt	50.5947	14.1128	Cenozoic	Tertiary (Paleogene-Tertiary)
NB26	Volcanic	Basalt	50.6178	14.3703	Cenozoic	Tertiary (Paleogene-Tertiary)
NB27	Volcanic	Basalt	50.6129	14.3572	Cenozoic	Tertiary (Paleogene-Tertiary)
NB28	Volcanic	Phonolite	50.5260	13.7639	Cenozoic	Tertiary (Paleogene-Tertiary)
NB29	Volcanic	Trachyte	50.5365	13.9177	Cenozoic	Tertiary (Paleogene-Tertiary)
NB30	Volcanic	Trachyte	50.5523	13.9282	Cenozoic	Tertiary (Paleogene-Tertiary)
NB31	Volcanic	Basalt	50.5307	14.0915	Cenozoic	Tertiary (Paleogene-Tertiary)
NB32	Volcanic	Basalt	50.5645	14.0891	Cenozoic	Tertiary (Paleogene-Tertiary)
NB33	Volcanic	Nephelinite	50.5648	14.1167	Cenozoic	Tertiary (Paleogene-Tertiary)
NB34	Volcanic	Basalt	50.5902	14.1501	Cenozoic	Tertiary (Paleogene-Tertiary)
NB35	Volcanic	Trachyte	50.5873	14.1826	Cenozoic	Tertiary (Paleogene-Tertiary)
NB36	Volcanic	Trachybasalt	50.6458	14.3098	Cenozoic	Tertiary (Paleogene-Tertiary)
NB37	Volcanic	Trachyte	50.6893	14.3056	Cenozoic	Tertiary (Paleogene-Tertiary)
NB38	Volcanic	Phonolite	50.6883	14.3323	Cenozoic	Tertiary (Paleogene-Tertiary)
NB39	Volcanic	Basalt	50.7024	14.3518	Cenozoic	Tertiary (Paleogene-Tertiary)
NB41	Volcanic	Basalt	50.7496	14.2680	Cenozoic	Tertiary (Paleogene-Tertiary)
NB42	Volcanic	Basalt	50.6882	14.4375	Cenozoic	Tertiary (Paleogene-Tertiary)
WB23	Volcanic	Nephelinite	49.8754	12.9799	Cenozoic	Tertiary (Paleogene-Tertiary)